Size Dependence of Stöber Silica Nanoparticle Microchemistry

Carlos A. R. Costa, Carlos A. P. Leite, and Fernando Galembeck*

Instituto de Química, Universidade Estadual de Campinas - UNICAMP. C. Postal 6154, CEP 13083-970, Campinas - SP, Brazil

Received: November 21, 2002; In Final Form: February 7, 2003

Five different samples of Stöber silica monodisperse particles show large variations in their swelling ability as well as on their chemical compositions. Nanosized particle diameters were determined under four different conditions, using suitable techniques: photon correlation spectroscopy (PCS) in water and ethanol, AFM at 25 °C under 55% relative humidity, high-resolution scanning electron microscopy and transmission electron microscopy, under 10^{-6} mbar. The comparison of these results shows that the smaller particles are highly swollen in ethanol, to a greater extent than in water. The swelling coefficients are lower for the larger particles, with a preference for water. Evidence for changes in the chemical composition were obtained by electron energy-loss and infrared absorption spectra: the smaller particles contain detectable amounts of C−H groups, which are not detected by IR in the larger ones, and O energy-loss spectra fine structure changes continuously with particle sizes. The location of carbon constituents in the particles was determined by electron spectroscopy imaging in the transmission electron microscope (ESI-TEM): they are dispersed throughout the finer particles, but they are excluded from the core of the larger particles. The results are interpreted considering the kinetics and extent of TEOS hydrolysis dependence on base concentration and the limiting effect of ethoxy residual groups on the densification of the silica network.

Introduction

Uniform fine particles are often used as model systems in the study of adsorption, catalysis, and size-dependent solid-state properties such as quantum confinement,[1] film formation, and particle self-arraying.[2,3] There have been significant achievements concerning the preparation of uniform colloid dispersions, both inorganic[4] and organic.[5] However, uniformity has often been considered only in relationship to particle size and shape, and little information is currently available concerning the uniformity of chemical composition of particles, even those made out using well-established procedures, such as the Stöber silica particles.

Many years ago, Stöber et al.[6] reported an elegant method for the preparation of monodisperse spherical silica particles with sizes covering almost the whole colloidal range, by tetraethyl orthosilicate (TEOS) hydrolysis, in ethanolic medium in the presence of ammonia. After this pioneering work, Stöber silica particles have been used as model colloids in a large number of experimental investigations.[7−10] Based on the Stöber method, Kaiser[11] prepared completely porous silica particles by cohydrolysis and subsequent condensation of tetraethoxysilane and a *n*-alkyltrialkoxysilane in a mixture of ethanol, water, and aqueous ammonia. Silica particles almost perfectly spherical with porous siliceous shells and dense cores were also obtained by Büchel and co-workers.[12] Preparation of spherical silica nanoparticles with a narrower size distribution than that obtained by hydrolysis of tetraethoxysilane in homogeneous alcoholic media has been achieved in microemulsion systems.[13−15]

Recently, several investigators have shifted their attention to the study of the mechanisms of formation and growth of these particles.[16] For this purpose, various techniques, such as nuclear magnetic resonance,[17] conductivity,[18] Raman scattering,[19] dynamic light scattering,[20] transmission electron microscopy,[21] and small-angle X-ray scattering,[22] were applied to investigate both the chemistry and the physical properties of the particles but, more noticeably, the kinetics of growth.[23] Thanks to these intensive investigations, an increasingly more complete picture for the formation of uniform silica particles is slowly emerging, but the elucidation of their domain nanostructure is an open and attractive research objective.

In this laboratory, we have recently observed significant heterogeneity and domain structure of polymer latex particles, which affects particle aggregation, macrocrystallization, and film formation.[24,25] This information is not usually available for inorganic fine particles, for which reason we decided to examine the uniformity of chemical composition of the Stöber silica particles. Two samples of particles of different sizes were previously examined,[26,27] using different imaging techniques. Large differences between the smaller and larger size particles were then observed, for which reason we decided to examine a larger array of samples, to gather more complete information on the particle microchemistry dependence on particle sizes.

Experimental Section

Preparation of the Silica Particles. Five different dispersions of silica nanoparticles (designated as A, B, C, D, and E) were prepared by the method of Stöber et al.[6] TEOS, absolute ethanol used as the solvent, and ammonium hydroxide were reagent grade. Glassware was cleaned with 10% hydrogen chloride and rinsed with distilled water and absolute ethanol. A total of 4 mL of TEOS were added to 50 mL of ethanol within screw-cap vials, in the presence of different amounts of NH_4OH (2, 2.5, 3, 3.5, and 4 mL respectively in samples A, B, C, D, and E) and placed within a water bath at (36 ± 0.1) °C under

* To whom correspondence should be addressed. Phone +55-19-3788-3080. Fax +55-19-3788-3023. E-mail: fernagal@iqm.unicamp.br.

10.1021/jp027525t CCC: $25.00
Published on Web 04/22/2003

ultrasonic vibration (25 kHz−200 W) for 120 min. Solid contents were determined gravimetrically on samples dried at 80 °C until constant weight (±0.2 mg).

Photon Correlation Spectroscopy (PCS). Effective diameter was measured in a ZetaPlus instrument (Brookhaven Instruments) with Bi-MAS software and a solid-state laser (15 mW, $\lambda = 670$ nm) as the radiation source. Samples were contained within 3-mL dust-free acrylic cuvettes. A volume of 100 μL of the silica dispersion was added to the cuvette previously filled with 2.5 mL of 10^{-3} M aqueous potassium chloride in order to give a suitable scattering intensity. The reported data are the averages of six individual runs on two sample aliquots.

Analytical Transmission Electron Microscopy Imaging. A Carl Zeiss CEM 902 transmission electron microscope, equipped with a Castaing-Henry energy filter spectrometer within the column and a Proscan Slow Scan CCD camera and controlled by a microcomputer running the AnalySis 3.0 system was used. The spectrometer uses inelastically scattered electrons to form energy-loss and element-specific images. When the electron beam passes through the sample, interaction with electrons of different elements results in characteristic energy losses. A prism-mirror system deflects electrons with different energies to different angles so that only electrons with a well defined energy are selected. If elastic electrons only are chosen ($\Delta E = 0$ eV), a transmission image with reduced chromatic aberration is obtained. When monochromatic inelastically scattered electrons are selected, electron spectroscopic images (ELSI) are formed, in which contrast is dependent on the local energy-loss spectrum and thus on the concentration fluctuations of a particular chosen element. Clear areas in the elemental distribution maps correspond to element-rich domains. The following procedure is used to acquire spectral images: a set of 38−42 images is acquired, around the absorption border for each element of interest. The energy window used is 6 eV, and the energy steps between images is 2.5 eV. This image set is used to define the three energy windows used for elemental mapping. Two images are recorded at energy windows below the absorption threshold, and they are used for fitting the background with a chosen function. The third image is obtained using an energy window set at the absorption band. The elemental map is obtained by subtracting the background from the image acquired in the third image, and it is checked for signal saturation, using the R-map macro from the AnalySis software. Each elemental map is validated by three independent checks: (i) contrast inversion in the plasmon region, (ii) spectral verification, and (iii) absence of signal saturation.

For individual silica particle examination, one drop of the silica dispersion was deposited on carbon-coated parlodion films supported in 400 mesh copper grids (Ted Pella). To make sure that the whole particles were not excessively thick, they were first observed using $\Delta E = 0$ eV electrons and then observed again at $\Delta E = 15-50$ eV. Image contrast inversion was always obtained, showing that a significant number of electrons were transmitted throughout the particles.[28] This observation is understood, considering that the 80 keV electrons mean free path within these silica particles is greater than 80 nm for elastic scattering[29] and is estimated as a few hundreds of nanometers, for inelastic scattering.[30]

Elemental images were observed for the relevant elements found in this sample, using the three-window technique,[31] with monochromatic electrons corresponding to the silicon K edge (1860 eV, 20 eV window), oxygen K edge (532 eV, 15 eV window) and carbon K edge (284 eV, 15 eV).

Image processing was performed in an IBM PC microcomputer using the Image-Pro Plus 4.0 image analyzer program (Media Cybernetics).

AFM Imaging. Silica dispersion droplets were allowed to dry on top of freshly cleaved mica surfaces, glued to the instrument sample holder for examination at room conditions. Noncontact AFM images were acquired using a TopoMetrix Discoverer instrument: the Si tip is matched at the natural frequency of mechanical oscillation. The tip is lowered to 10 nm of the sample surface. The mechanical oscillation of the tip is tracked by a four-quadrant photodetector and analyzed by a feedback loop to control the distance between tip and sample surface, while scanning the sample at constant oscillation amplitude. The topographic image is built pixel by pixel, using the voltage fed to the z piezoelectric ceramic by the loop.

FESEM Imaging. The samples were prepared as follows: a droplet of silica dispersion was placed on top of a freshly cleaved mica surface (previously glued to the flat surface of a brass stub) and allowed to dry at room conditions. Dry samples were coated with a thin carbon layer (15 nm). A JEOL JSM-6370F field emission scanning electron microscope was used. The nominal resolution of this instrument is 3 nm, when it is operated at 15 kV and using a 70 μm aperture.

Infrared Spectra. Infrared spectra were acquired in a Bomem B-100 spectrometer, from particle films cast from the dispersions on BaF_2 windows, and dried for 20 min under a 47.5% relative humidity (RH), at 19 °C.

Electron Energy Loss Spectra (EELS). EELS in the 520−590 eV range were acquired in the CEM-902 transmission electron microscope used for imaging, by the parallel acquisition method. The acquisition time necessary to obtain a good signal-to-noise ratio is 3 s for the oxygen K edge spectrum, with an objective aperture size of 90 μm.

Results

The solid contents of all preparations were gravimetrically determined after 24 h aging, and they were in the 2.5 (sample E) to 2.7 (sample A) weight percent range. The expected figures for dry SiO_2 sol content calculated from the amount of TEOS used are 2.3−2.4%, showing that the yield calculated as (weight of solid product/ theoretical weight of dry silica) exceeds 100%, what can only be possible if the reaction proceeds close to completion and the product is a hydrous silica. PCS particle size measurements were made after 1 day, 1 week, and 13 months, in the ethanolic sol, and the results were constant within experimental error, which confirms the exceptional stability of these sols, in agreement with the literature.[32] Particle sizes were determined for all five samples, under five different conditions: PCS measurements in ethanol as well as in water, AFM microscopy under room conditions (55% RH, 25 °C), TEM, and FESEM (both under high vacuum, better than 10^{-6} mbar). The morphological and aggregation characteristics of the particles changed with size, as presented in Figures 1−3. A general trend is clearly observed: the smaller particles tend to aggregate stronger than the larger ones, and they are more extensively deformed from the presumed originally spherical shapes, in liquid dispersion. This renders size measurements more difficult and uncertain, because the larger aggregates cannot be used for this purpose.

The particle diameters determined by the various techniques are summed up in Table 1, and they show many interesting features:

(1) Particles appear paucidisperse in all techniques used; most standard deviations are in the 1−10% range.

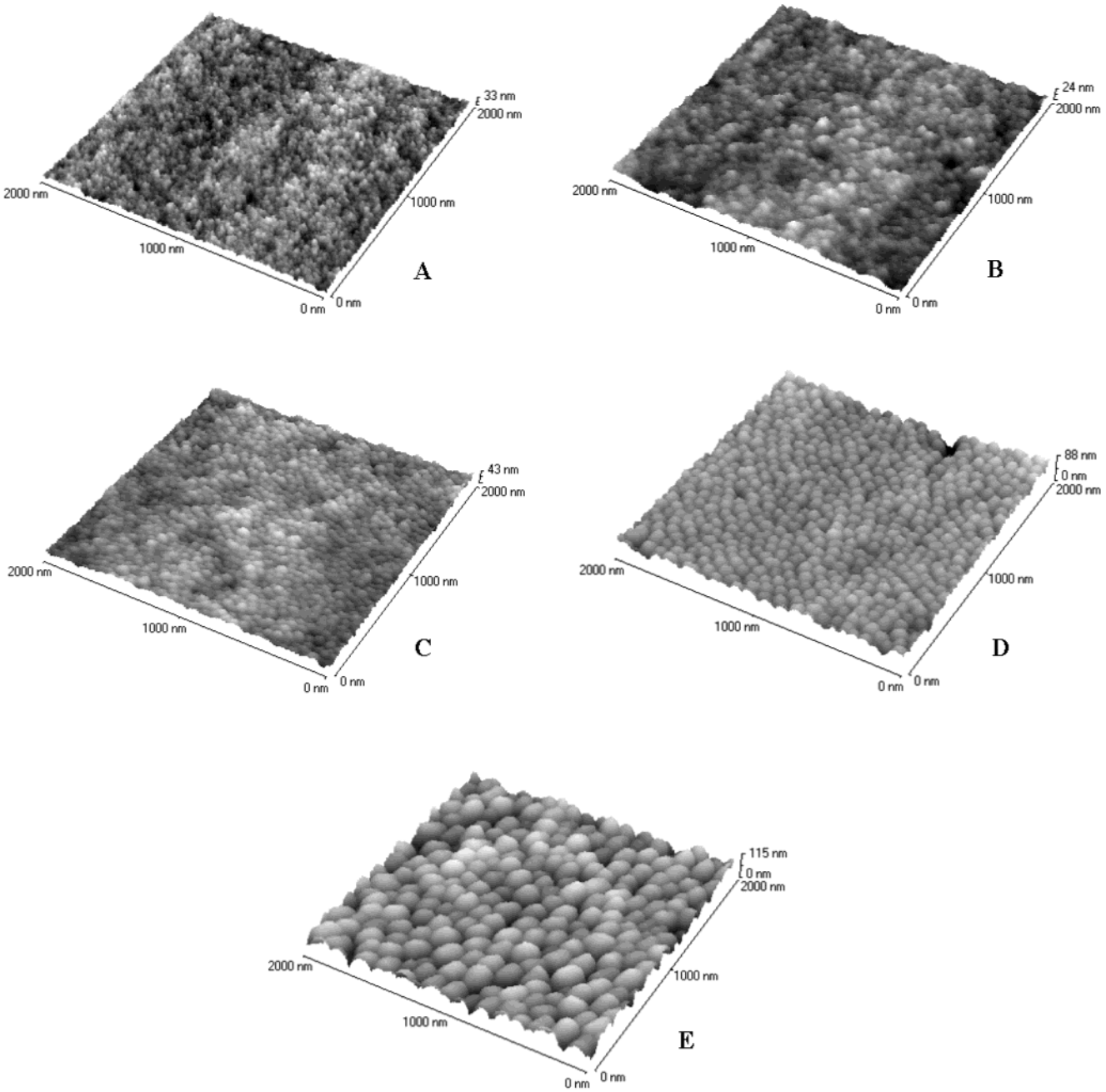

Figure 1. AFM images of Stöber silica particle films. Film thickness, 8 μm. The sample designations (from A to E) are the same as in Table 1.

(2) Particle effective diameters determined by PCS are significantly larger than those determined by AFM, SEM, or TEM, pointing toward a strong particle swelling or chain expansion at the particle surfaces, as in the "hair" formation described by Hunter in the case of polymer lattices.[33]

(3) The differences between the measurements under liquid, under air, or under high vacuum are very large especially in the case of the smaller particles.

(4) The difference between the small particle diameters by PCS and AFM is very large, showing that there is significant particle shrinking even without exposing them to vacuum or electron beam heating.

(5) The two smaller particle samples show larger effective diameters in ethanol than in water, whereas the other three show larger diameters in water.

(6) The measurements by SEM always produce larger values than those made by TEM, which is understood considering that the particles were carbon-coated for SEM observation but not for TEM, and the carbon coating reaches a few nanometers, at least.

(7) The difference between AFM and SEM measurements is also significant, meaning that dry particles still undergo dehydration as the samples are taken out of the room environment and transferred to vacuum.

These particle size measurements show that the small particles are more highly swollen than the larger ones, and they swell more in ethanol than in water, whereas the larger particles swell more in water than in ethanol. Swelling coefficients are strongly dependent on the chemical nature of the involved phases; thus, the particle size measurements provide strong evidence in favor of the hypothesis of a change in particle chemical composition, with particle size.

This was verified by measuring the infrared spectra of thin films prepared by drying the ethanol particle dispersions on BaF_2

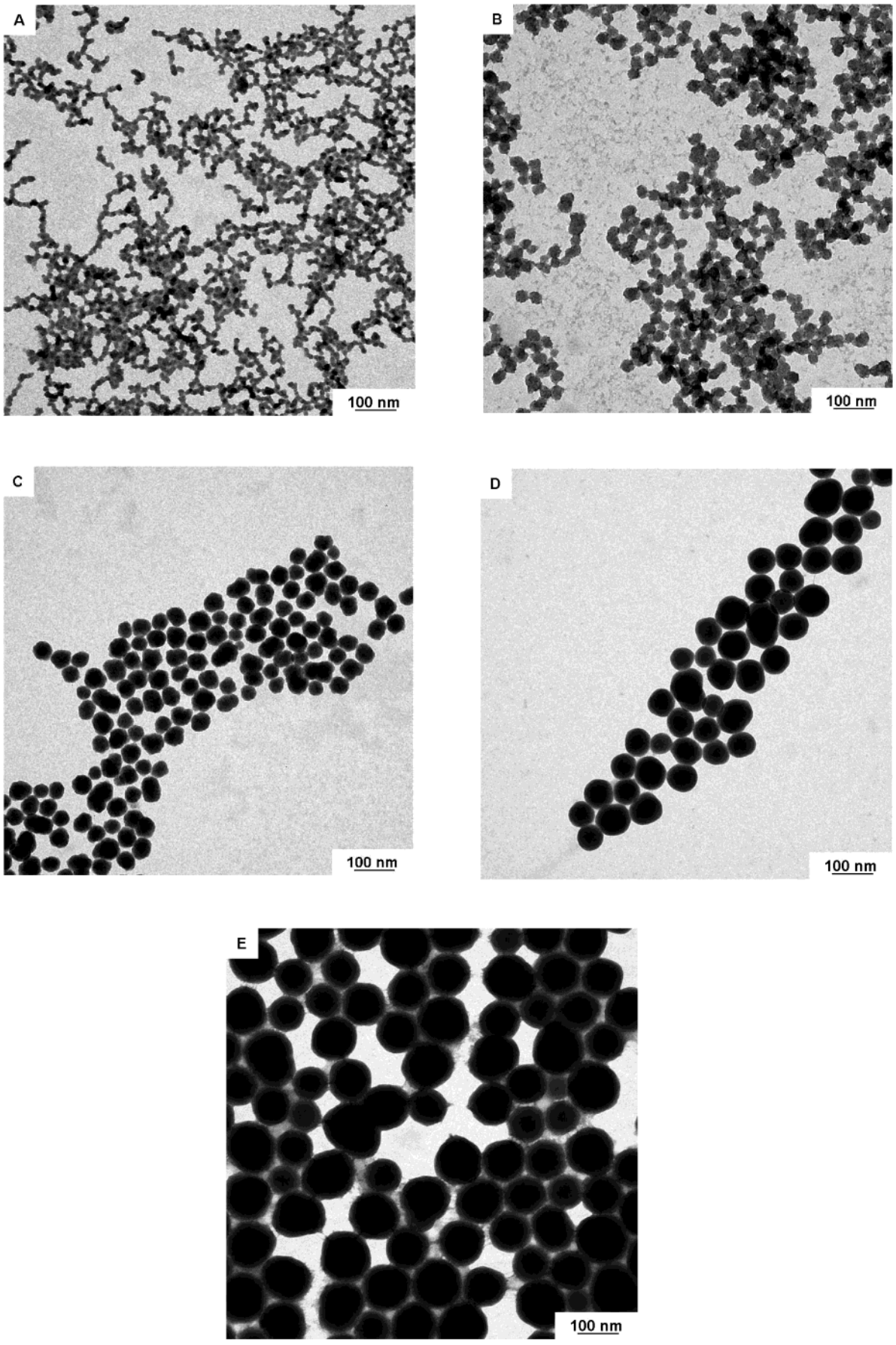

Figure 2. Bright-field TEM micrographs of silica particle submonolayers. The sample designations (from A to E) are the same as in Table 1.

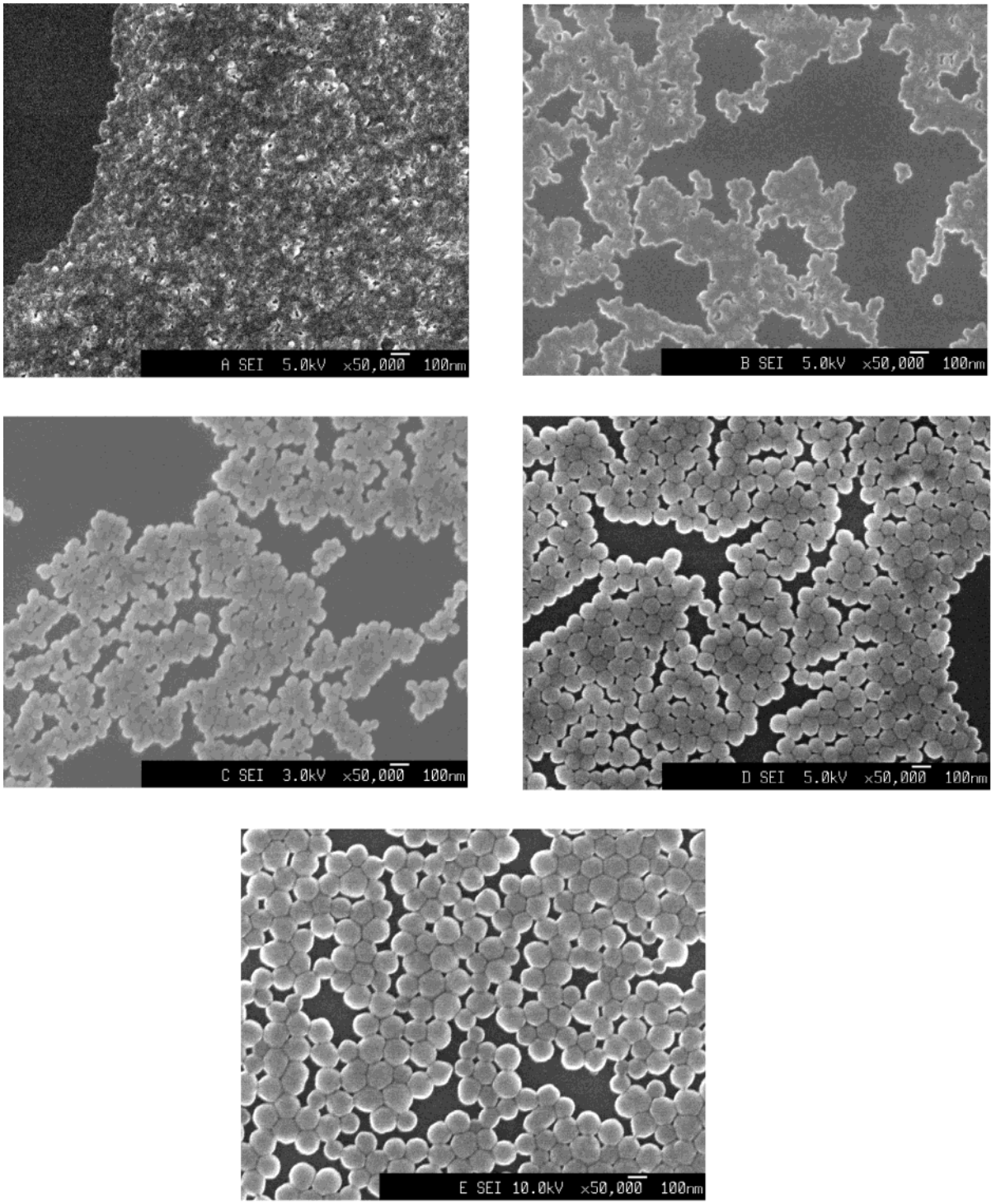

Figure 3. SEM images of Stöber silica particle submonolayers. The sample designations (from A to E) are the same as in Table 1.

windows. The spectra are given in Figure 4, and they differ from one to another sample.

The main observations from these spectra are as follows:

(1) The films prepared with the smaller particles show a small but definite peak at 3000−2900 cm^{-1}, showing that they contain detectable amounts of C−H groups. This peak is not seen in the larger samples.

(2) The absorbance ratios of the peaks assigned to Si−OH stretching (3200−3600 cm^{-1}) and to Si−O−Si deformation (1100−1000 cm^{-1}) decrease from the smaller to the larger samples, showing that the latter are less hydrated than the former.

To sum up, from the infrared spectra, we conclude that the smaller particles are more hydrous and more strongly ethoxylated than the larger ones, or else, the larger particles chemical composition is closer to SiO_2 than the smaller ones.

Another important question is the distribution of the carbon constituents throughout the particles from the five samples. This was addressed by acquiring the carbon distribution elemental maps, which are presented in Figure 5.

The differences between the different maps are striking:

(1) The particle aggregates from the smaller sample (A) appear brighter than the background, which has a contribution from the carbon-parlodion supporting film. Consequently,

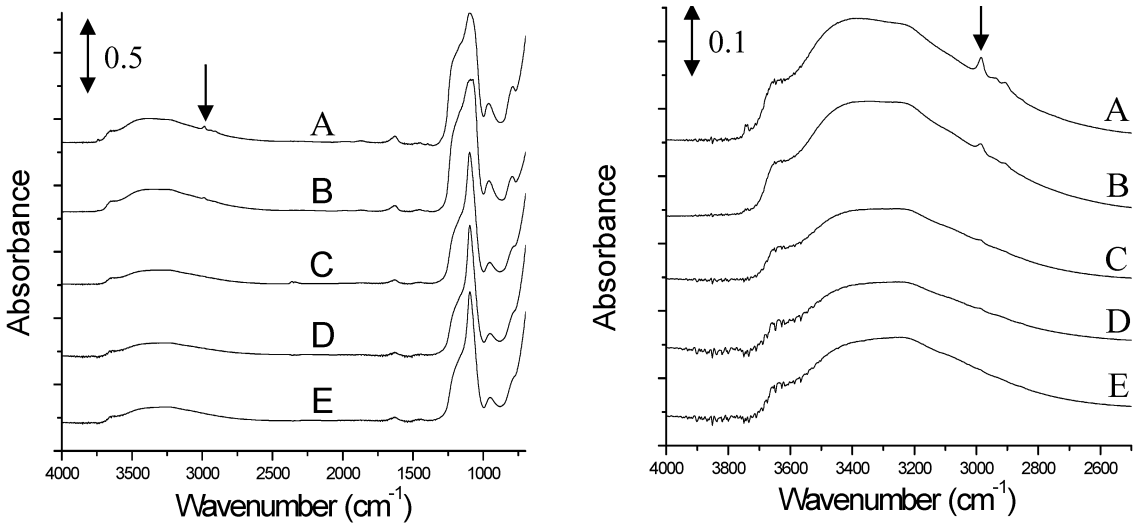

Figure 4. IR absorption spectra of thin films of silica. Samples A−E are the same as in Table 1. The arrows indicate the peak assigned to C−H stretching vibration (3000−2960 cm^{-1}).

TABLE 1: Particle Size Determination by PCS (in Water and Ethanol), AFM, SEM, and TEM, for the Silica Particle Samples

sample environment during the measurement	technique	sample (amount of ammonia used during sample preparation, mL) A (2)	B (2.5)	C (3)	D (3.5)	E (4)
water, 25°C	PCS (nm)	54 ± 5	66 ± 6	77 ± 2	103 ± 1	136 ± 1
ethanol, 25°C	PCS (nm)	72 ± 2	74 ± 2	67 ± 6	99 ± 1	131 ± 1
air, 55% RH, 25°C	AFM (nm)	33 ± 2	45 ± 4	57 ± 5	81 ± 8	125 ± 11
10^{-6} mbar	FESEM (nm)	22 ± 2	39 ± 3	51 ± 4	79 ± 7	118 ± 10
10^{-6} mbar	TEM (nm)	15 ± 2	33 ± 3	47 ± 4	76 ± 7	115 ± 10
Apparent volume increase in water (%)		4600	700	340	149	65
Apparent volume increase in ethanol (%)		11000	1028	190	121	48
Solids content (% w)		2.7	2.7	2.6	2.5	2.5
Zeta potential (mV), KCl 10^{-3}M		−27	−38	−36	−46	−49

carbon contents in the particles are comparable to a carbon film with a few nanometers thickness.

(2) The larger particles (samples C, D, and E) appear darker than the background, evidencing that they contain smaller amounts of the carbon compounds. On the other hand, interparticle interstices in C are very bright, showing the presence of a significant amount of carbon compounds in the particle shell layers. This is also observed but less markedly, in particles D and E.

(3) Sample B particles show the coexistence of highly contrasting domains, but these appear randomly distributed throughout the particles.

(4) The background of the A sample map also shows a marked contrast created by elongated small bright spots, which are likely nonparticulate compounds containing carbon. Contrast in the background of C maps is also perceived in the other samples but less markedly, and it is hardly noticed in the Si and O maps shown in Figures 6 and 7.

The O and Si elemental maps were acquired for all five samples, and they follow our earlier observations. However, because we have now a more sensitive camera and an upgraded image acquisition system, we can observe that not only the particles in the O maps appear larger than in the Si maps, but also they display elongated structures protruding out of the surface, which are less clearly visible in the Si maps. The definition of the particle surfaces is much better in the Si maps than in the O maps, and this is understood considering that the outermost surface layers and the protrusions are made out of ethoxylated silicic acid, with a higher O/Si ratio than the particle bulk.

A final evidence for the gradual changes among the five different samples comes from the electron energy loss spectra in the oxygen threshold, presented in Figure 8.

The fine structure of an energy loss spectrum depends on the chemical environment for the respective element; consequently, we observe a gradual change in the distribution of O chemical environments, with the sample size. As of now, the identity of the environments is not possible, because of the lack of reference data, in the literature.

Discussion

Previous work from this laboratory supported the following picture for the Stöber silica particles: the smaller ones are made out of mixed domains with variable Si/O ratios, whereas the larger ones have a core-and-shell structure, and the shell is more hydrous than the particle core. Now, we observe that the transition between these two kinds of domain arrangements proceeds gradually, from the smaller to the larger particles. Moreover, the carbon constituents (from ethoxy groups) pattern of topochemical distribution also changes gradually, from a great degree of superimposition to the Si- and O-rich domains to an almost complete exclusion from the larger particles, in which carbon constituents seem rather restricted to the particle surfaces. Consequently, the actual topochemistry of silica nanoparticles is quite different from that found by Iler[34] for most silica sols, as discrete spherical particles of amorphous anhydrous silica with a 2.2 g cm^{-3} density.

The present results show that the silica particles have a pronounced domain structure but the larger particles have also a higher C content and a higher O/Si ratio at the particle borders, as compared to the particle cores. The thickness of the shell layer extends for many nanometers.

Following existing reports on silica particle formation from TEOS, carbon from the ethoxy groups is transformed into ethanol, which is easily dialyzed and also lost by evaporation.[12]

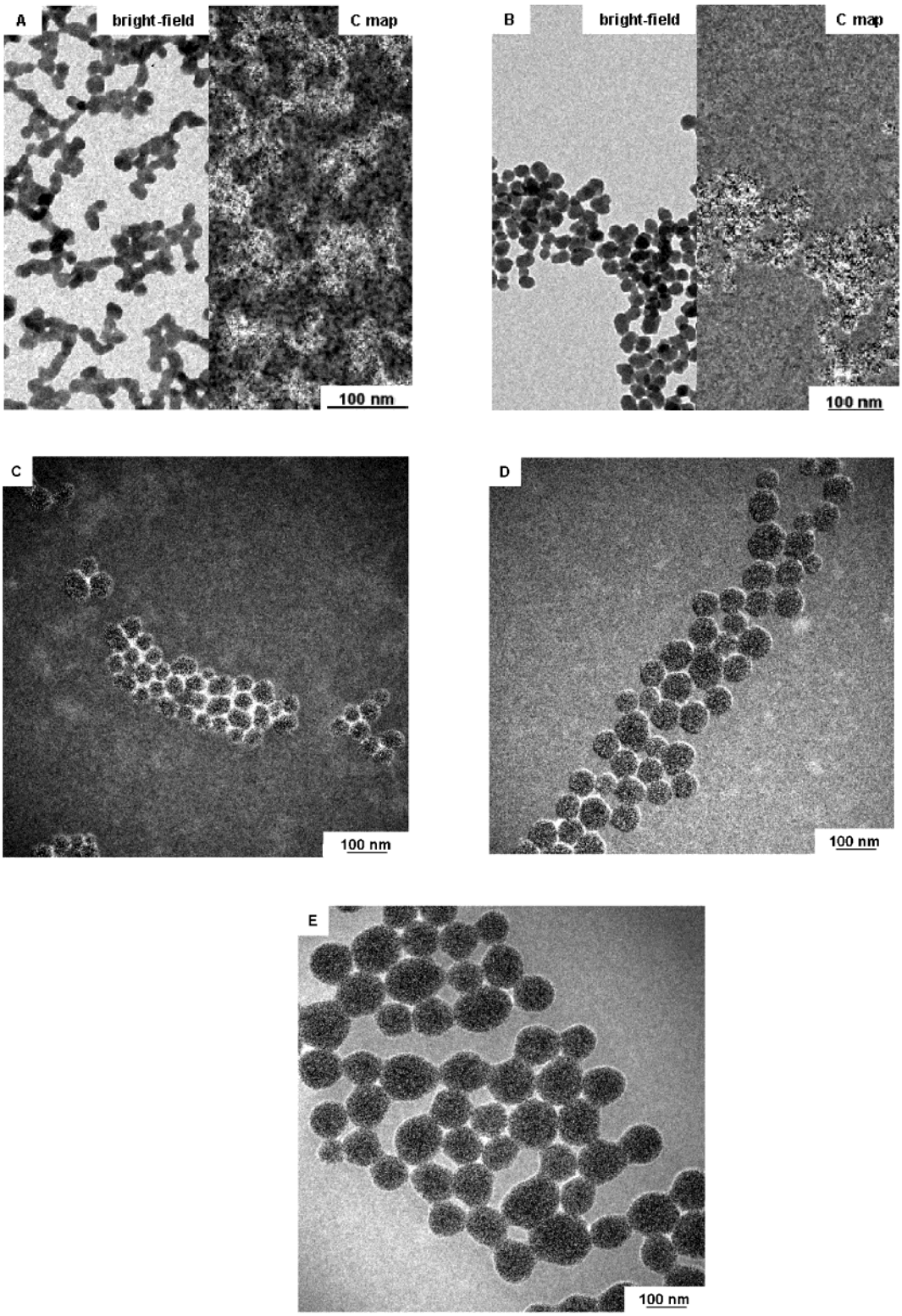

Figure 5. Carbon distribution elemental maps (ESI-TEM) of Stöber silica particle submonolayers. The sample designations (from A to E) are the same as in Table 1. The carbon maps for samples A and B are given side by side with the corresponding bright field images, to facilitate the observation of the discontinuity of C-rich domains within the particles.

However, Van Helden et al.[7] have already reported the presence of carbon in the composition of Stöber silica particles. They assumed that the carbon content determined gravimetrically originates from unhydrolyzed ethoxy groups and calculated that the particles contain 91.5% weight silica, 5.25% water, and 0.97% ethoxy groups. Now, the observation of carbon compounds in the particle shells as well as in the background and in the interparticle interstices shows that carbon content and also carbon distribution in the particles is size-dependent. To sum up, the smaller particles (samples A and B) examined in this work differ markedly from the larger (samples C, D, and E) particles in Si, O, and also C distribution.

The domain structure of the larger and smaller particles as well as the core-and shell nature of the former may be

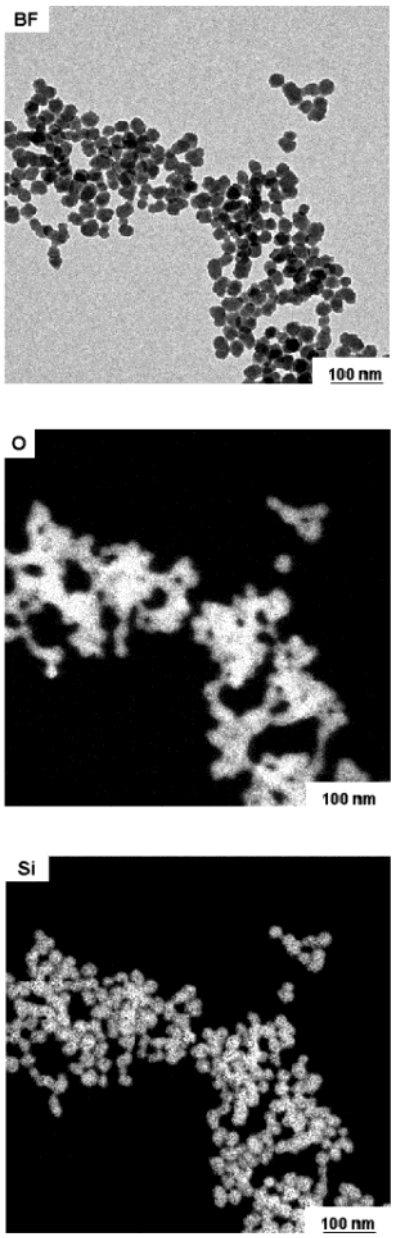

Figure 6. Bright-field micrograph, O and Si elemental maps for sample B.

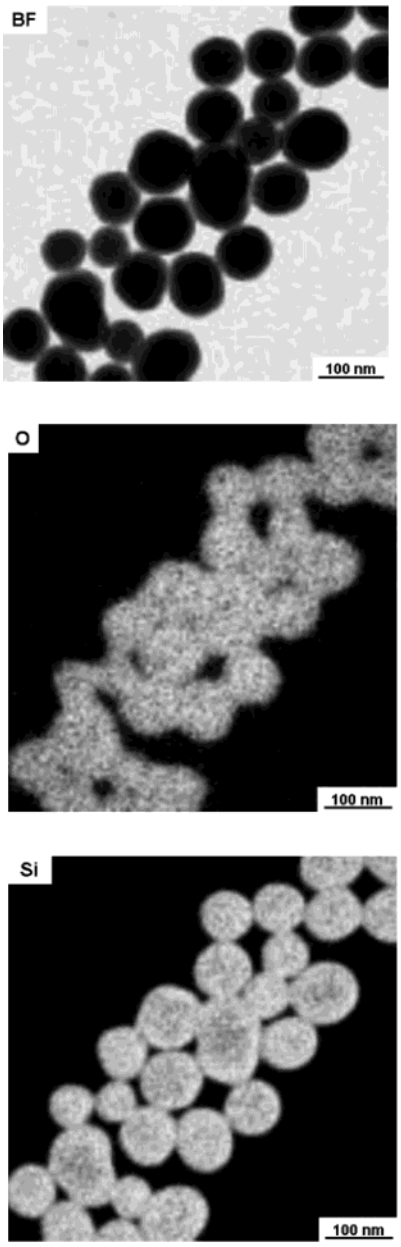

Figure 7. Bright-field micrograph, O and Si elemental maps for sample D.

understood considering the particle synthesis procedure and the intervening ethoxy group hydrolysis and silanol condensation reactions.[23,35−37] Using the results of cryo-TEM experiments, Bailey and Mecartney[21] postulated that hydrolyzed monomer polymerizes to form microgel clusters due to polysilicic acid cross-linking that collapse upon reaching a certain size and cross-linking density. Following the present results, the collapse of the (smaller, highly swelling) particles prepared using lower ammonia concentrations is prevented by the persistence of greater amounts of non-hydrolyzed ethoxy groups. Seed particle growth is thus inhibited by incomplete hydrolysis, because of a decrease in the rate of growth of the silicic acid polymers. Other elaborate particle formation mechanisms were proposed in the literature, concerned with the fractal nature of the particles[16] and the dependence of the formation of highly branched clusters[38] on the base-catalyzed reactions, but these should be further revised considering the present evidence for the chemical differences between particles prepared using different base concentrations, derived from ethoxy residues.

The persistence of ethoxy groups distributed throughout the smaller particles and evidenced in the IR and EELS spectra explains their strong swelling behavior in ethanol, in analogy to the well-known silicone rubber swelling ability in this solvent.[39] Moreover, these groups decrease the connectivity of the polysilicic acid chains thus preventing the densification of the silica network and leaving also a greater proportion of noncondensed silanol groups, which contribute to their swelling in water.

Under higher ammonia concentrations, ethoxy replacement by hydroxo groups is more complete, and the silanol condensation reactions are thus allowed to a greater extent, decreasing the particle swelling ability both in water and in ethanol. The larger particles show lower swelling coefficients, and they swell more in water than in ethanol, because the main groups responsible for interaction with solvent are now the silanol groups, instead of ethoxy groups.[40]

From the micrographs presented in this work, particle packing in the dry films is clearly more effective in the case of the

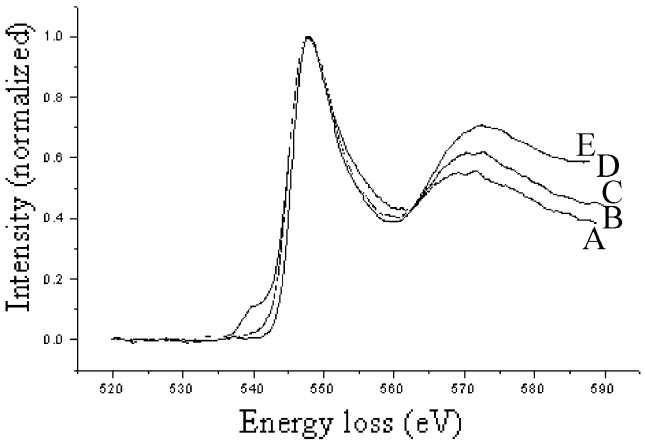

Figure 8. Electron energy loss spectra around the oxygen K level threshold. For the sake of comparison, the spectra were normalized using the 547 eV peak as the reference. The sample designations (from A to E) are the same as in Table 1.

smaller particles. This may now be easily understood, considering that the smaller particles are less densely cross-linked and they are also strongly plasticized by the swelling solvents. They also have a lower zeta potential modulus, and consequently, they can approach, deform, and pack more easily than the larger particles, when the films are cast.

Conclusions

Stöber silica particles from different sizes are widely different concerning their chemical compositions and swelling behavior in the presence of water and ethanol: the smaller particles prepared in the presence of lower concentrations of base contain broadly distributed residual ethoxy groups that limit silicic acid chain extension and cross-linking, thus limiting particle growth in the dispersion but making the smaller particles more strongly swollen by ethanol and water. Drying the smaller particles dispersion produces densely packed films, because of their higher plasticity arising from solvent retention and a lower degree of cross-linking.

Acknowledgment. The authors thank FAPESP, Pronex/Finep/MCT, and CNPq. This is a contribution from the Millenium Institute for Complex Materials.

References and Notes

(1) Henglein, A. *Chem. Rev*. **1989**, *89*, 1861.
(2) Averback, R. S.; Höfler, H. J.; Tao, R. *Mater. Sci. Eng*. **1993**, *166*, 169.
(3) Galembeck, F.; Lima, E. C. O.; Masson, N. C.; Monteiro, V. A. R.; Souza, E. F. In *Fine Particles Science and Technology: From Micro to Nanoparticles*; Pelizzetti, E., Ed.; Kluwer: Dordrecht, 1996; p 267−279.
(4) Matijevic, E. *Chem. Mater*. **1993**, *5*, 426.
(5) Hammouda, A.; Gulik-Krzywicki, T.; Pileni, M. P. *Langmuir* **1995**, *11*, 3656.
(6) Stöber, W.; Fink, A.; Bohn, E. *J. Colloid Interface Sci*. **1968**, *26*, 62.
(7) Van Helden, A. K.; Vrij, A. *J. Colloid Interface Sci.* **1980**, *78*, 312.
(8) Kirkland, J. J. J. *Chromatogr*. **1979**, *185*, 273.
(9) Kops-Werkhoven, M. M.; Fijnaut, H. M. *J. Chem. Phys*. **1981**, *74*, 1618.
(10) Tan, C. G.; Bowen, B. D.; Epstein, N. *J. Colloid Interface Sci.* **1987**, *118*, 290.
(11) Kaiser, C.; Büchel, G.; Lüdtke, S.; Lauer, I.; Unger, K. K. In *Characterisations of Porous Solids IV*; McEnaney, B., Mays, T. J., Rouquérol, J., Rodríguez-Reimoso, F., Sing, K. S. W., Unger, K. K., Eds.; Royal Society of Chemistry: Cambridge, U.K., 1997; p 406−412.
(12) Büchel, G.; Unger, K. M.; Matsumoto, A.; Tsutsumi, K. *Adv. Matter*. **1998**, *10*, 1037.
(13) Osseo-Asare, K.; Arriagada, F. J. *Colloids Surf.* **1990**, *50*, 321.
(14) Minehan, W. T.; Messing, G. L. *Colloids Surf.* **1992**, *63*, 181.
(15) Esquena, J.; Tadros, Th. F.; Kostarelos, K.; Solans, C. *Langmuir* **1997**, *13*, 6400.
(16) Boukari, H.; Lin, J. S.; Harris, M. T. *Chem. Mater*. **1997**, *9*, 2376.
(17) Lee, K. T.; Look, J. L.; Harris, M. T.; McCormick, A. V. *J. Colloid Interface Sci*. **1997**, *194*, 78.
(18) Bogush, G. H.; Zukoski, C. F. *J. Colloid Interface Sci*. **1991**, *142*, 1.
(19) Matsoukas, T.; Gulari, E. *J. Colloid Interface Sci.* **1988**, *124*, 252.
(20) Biddle, D.; Walldal, C.; Wall, S. *Colloids Surf., A* **1996**, *118*, 89.
(21) Bailey, J. K.; Mecartney, M. L. *Colloids Surf., A* **1992**, *63*, 151.
(22) Konishi, T.; Yamahara, E.; Ise, N. *Lagmuir* **1996**, *12*, 2608.
(23) Boukari, H.; Lin, J. S.; Harris, M. T. *J. Colloid Interface Sci*. **1997**, *194*, 311.
(24) Cardoso, A. H.; Leite, C. A. P.; Galembeck, F. *Langmuir* **1998**, *14*, 3187.
(25) Galembeck, F.; Souza, E. F. In *Polymer Interfaces and Emulsions*; Esumi, K., Ed.; Marcel Dekker: New York, 1999; p 119−166.
(26) Costa, C. A. R.; Leite, C. A. P.; Souza, E. F.; Galembeck, F. *Langmuir* **2001**, *17*, 189.
(27) Leite, C. A. P.; Souza, E. F.; Galembeck, F. *J. Braz. Chem. Soc.* **2001**, *12*, 519−525.
(28) We are grateful to Dr. W. Probst (LEO-Zeiss Elektronenmikroskopie Gmbh) for this valuable private communication.
(29) Newbury, D. E. In *Principles of Analytical Electron Microscopy*; Joy, D. C., Romig, A. D., Jr., Goldstein, J. L., Eds.; Plenum Press: New York, 1986.
(30) Newbury, D. E. In *Principles of Analytical Electron Microscopy*; Joy, D. C., Romig, A. D., Jr., Goldstein, J. L., Eds.; Plenum Press: New York, 1986; p 20.
(31) Reimer, L.; Zepke, U.; Moesch, J.; Schulze-Hillert, St.; Ross-Messemer, M.; Probst, W.; Weimer, E. *EELS Spectroscopy: A Reference Handbook of Standard Data for Identification and Interpretation of Electron Energy Loss Spectra and for Generation of Electron Spectroscopic Images*; Carl Zeiss: Oberkochen, 1992.
(32) Kiraly, Z.; Turi, L.; Dekany, I.; Bean, K.; Vincent, B. *Magyar Kemiai Folyoirat* **1995,** *101*, 501.
(33) Midmore, B. R.; Hunter, R. J. *J. Colloid Interface Sci.* **1988**, *122*, 521.
(34) Iler, R. K. *The Chemistry of Silica*; Wiley: New York, 1979.
(35) Lindberg, R.; Sjöblom, J.; Sundholm, G. *Colloids Surf., A* **1995**, *99*, 79.
(36) Harris, M. T.; Brunson, R. R.; Byers, C. H. *J. Non-Cryst. Solids* **1990**, *121*, 397.
(37) Bogush, G. H.; Zukoski, C. F. In *Ultrastructure Processing of Advanced Ceramic*; Mackenzie, J. D., Ed.; Wiley: New York, 1988; p 477.
(38) Yamane, M.; Inoue, S.; Yasumori, J. *J. Non-Cryst. Solids* **1984**, *63*, 13.
(39) Goncalves, M. D.; Marques, G. D. S.; Galembeck, F. *Separ. Sci. Technol.* **1983**, *18*, 893.
(40) Galembeck, F.; Costa, C. A. R.; Leite, C. A. D. *Abstr. Pap. Am. Chem. S.* **2002**, *224*, 042.